JOURNAL OF CATALYSIS 6, 288–307 (1966)

Conversion of Parahydrogen to Orthohydrogen Using Nickel / Alumina Catalysts

W. R. ALCORN* AND T. K. SHERWOOD

From the Massachusetts Institute of Technology, Cambridge, Massachusetts

Received May 10, 1966; revised June 13, 1966

The para–ortho hydrogen conversion was studied with both powdered and pelleted nickel/alumina catalysts in a continuous-flow system in the range 25–65°C and 0.15–0.95 atm. Results were compared with kinetic models developed by the steady state method using several postulated mechanisms. The observed reaction kinetics were consistent with a number of mechanisms, and the overall kinetics with the pellets were consistent with a simple pore-diffusion model. Activation energies for five powder catalysts fell in the unusually wide range of 1.6 to 10.4 kcal/mole and showed a compensation effect.

NOMENCLATURE

A	Frequency factor; $K_0 = Ae^{-E/RT}$ (cm³/sec g)
A_p	Superficial catalyst pellet area for mass transfer (cm²)
c_m, c_{mo}, c_{mp}, c_{mt}	Surface concentrations of empty sites, o-H_2, p-H_2, total sites ($c_{mt} = c_m + c_{mo} + c_{mp}$)
c_o, c_p, c_t	Bulk gas concentrations of o-H_2, p-H_2, total H_2 ($c_t = c_o + c_p$) (moles/cm³)
c_{oe}, c_{pe}	Bulk gas concentrations of o-H_2, p-H_2 at equilibrium at reactor temperature (moles/cm³)
c_{ps}	Gas concentration of p-H_2 adjacent to external catalyst surface (moles/cm³)
D_B	Molecular (bulk) diffusivity (cm²/sec); here, self-diffusivity of H_2
D_{eff}	Effective diffusivity in pellet, based on area A_p (cm²/sec)
E	Apparent activation energy (kcal/mole)
k_c	Mass-transfer coefficient (cm/sec)
k_c'	Pressure-independent part of k_c ($k_c' = k_c c_t$) (moles/cm² sec)
K_0	Overall rate coefficient (cm³/sec g)
K_r	Reaction rate coefficient (cm³/sec g)
L	Half-thickness of pellet (cm)
Q	Volumetric flow rate through reactor (cm³/sec)
r	Reaction rate (moles/sec)
W	Catalyst weight (g)
y_p, y_{pe}	Gas mole fractions corresponding to c_p, c_{pe}
η	Effectiveness
η_p	Pellet density (g/cm³)
τ	Tortuosity
ϕ	Modified Thiele modulus

* Presently at Leesona Moos Laboratories, Great Neck, Long Island, New York.

INTRODUCTION

Though not known to be of technical importance, the conversion of para- to ortho-hydrogen at moderate temperatures has been found to be a powerful tool in understanding catalytic reactions involving hydrogen, and offers promise as a standard reaction for use in evaluating chemical and physical catalyst factors. The stoichiometry of the reaction is simple and the enthalpy change at room temperature and above is so small that temperature gradients in the gas–catalyst

system are negligible. The present study is concerned with the heterogeneous chemical conversion at 25° to 65°C, well below the temperature range of 400° to 500°C, at which homogeneous gas-phase conversion becomes important. The objectives were two: to establish the reaction kinetics on nickel/alumina powder, and to use the reaction as a tool for studying pore-diffusion effects with pellets made by compacting the same powder.

The catalytic conversion of para- to ortho-hydrogen has been studied extensively, using metal wires, foils, tubes, powders, and films, and with oxides, salts, and glass. Results are reported for a wide range of temperatures and pressures, most of the data being obtained using batch reactors at constant total pressure. The data up to about 1960 on metal catalysts are reviewed by Bond (*1*). Activation energies found with transition metals range from 0.5 to 10.6 kcal/mole; the range for nickel is 1.4 to 10.6 kcal/mole. The *sp* metals showed activation energies from 0.3 to 23.1 kcal/mole.

The one finding common to all of the published studies is that the reaction rate at constant temperature and total pressure is proportional to concentration of reactant in excess of its equilibrium concentration. Thus for conversion of p-H_2(g) to o-H_2(g) the rate r in moles/sec at T and P is given by

$$r = K_0W(c_p - c_{pe}) = (K_0WP/RT)(y_p - y_{pe}) \quad (1)$$

where W is the catalyst mass in grams, c_p is the ambient p-H_2 concentration, moles/cm^3; c_{pe} is the equilibrium p-H_2 concentration, y_p and y_{pe} are the mole fractions corresponding to c_p and c_{pe}, and K_0 is an "overall rate coefficient." The last, which is a function of T and P, becomes equal to a "reaction rate coefficient," K_r, if mass-transfer resistances are absent. K_0 and K_r have units of cm^3/(sec) (g catalyst).

The variation of conversion with pressure has been described in nineteen or more published investigations. Earlier workers reported the reaction to be of various "orders"; most later workers found that for a given catalyst at constant temperature K_0 was inversely linear in P, whence

$$r = W(c_p - c_{pe})/A(1 + BP) \quad (2)$$

where A and B are experimentally determined constants. Thus the "order" of the reaction may fall between zero and unity, depending on the pressure and the values of A and B. Equation (2) has been found to apply to conversion with supported catalysts, metal wires, metal films, and to both transition and *sp* metals.

Reaction mechanism. The mechanistic schemes so far proposed are variations of two basic types. They are listed in Table 1 along with some additional schemes representing plausible extensions of the others. In the Bonhoeffer-Farkas mechanisms hydrogen molecules adsorb on the surface and dissociate; the atoms then recombine in the equilibrium ortho–para ratio and desorb. In the Rideal-Eley mechanisms there is interaction between two species: one strongly adsorbed, probably atomic, and one either weakly adsorbed (chemically or physically) or impinging directly from the gas phase. The Bond variation, involving types A and C hydrogen, is similar to the Eley scheme. Boreskov and Vassilevitch (*3*) incorporate the concept of surface migration between sites of different adsorption strengths.

The several mechanisms are discussed by Bond (*1*) and by Eley (*9*). The Eley (or Bond, or Boreskov) mechanisms appear to be applicable to the transition metal catalysts in view of the strong evidence of adsorption of two or more hydrogen species on the surface. The Bonhoeffer-Farkas (or Schwab) mechanisms appear most plausible for sparsely covered surfaces such as the *sp* metals, or transition metals at high temperatures.

Kinetic analysis. Several authors have shown that the kinetics of the conversion, as represented by Eq. (2), can be derived with Langmuir-Hinshelwood kinetics, i.e., a model involving the sequence of adsorption, surface reaction, and desorption, and the assumption of adsorption–desorption equilibrium. Of the mechanisms listed in Table 1, only the "Schwab" variation is strictly consistent with the model. Eley and Shooter (*9*) compared a number of mechanisms with kinetic data on the basis of a modified Langmuir-Hinshelwood approach, and concluded

that in addition to the Bonhoeffer-Farkas single-site mechanism (here listed as Schwab), the "Eley" mechanism (Table 1) is consistent with Eq. (2). On the same basis, they rejected the original Bonhoeffer-Farkas and the second Rideal mechanisms because they would imply a $P^{1/2}$ term in the kinetic equation.

The steady state method (*4*, *15*) allows more freedom in choosing the mechanistic models, and includes Langmuir-Hinshelwood kinetics as a special case. The basic assumption, that intermediate surface concentrations are constant with time, appears satisfactory for the present study of a relatively slow reaction in a steady-flow reactor with minimal catalyst activity change. Table 1 lists the reduced kinetic equations obtained by applying the steady state method to the tabulated mechanisms. Equations (3) and (4) are derived in the Appendix, where it is shown that the first (single-site, or Schwab) result is identical to that obtained by the Langmuir-Hinshelwood method if it is assumed that the surface conversion step is rate-determining.

It is assumed in the Rideal-Eley mechanisms that the surface has a fixed concentration of strongly adsorbed atomic hydrogen which remains constant though taking part in the reaction. Thus the reason that each Rideal-Eley mechanism is mathematically equivalent to a Bonhoeffer-Farkas mechanism is that the latter's open site (M) is analogous to a partly filled site pair $\binom{\mathrm{H}}{\mathrm{MM}}$ in the former. However, the equivalence is only mathematical, since the coefficients have different meanings in the two cases. It should be noted that the derivations are based on concentrations, and that the total pressure is the sum of the partial pressures obtained from the concentrations of ortho- and parahydrogen. The linear effect of P indicated by Eq. (2) would not be expected if an inert gas were present.

The first four sets of mechanisms can be expressed by a rate equation of the form $r = WK_r(c_\mathrm{p} - c_\mathrm{pe})$, where

$$1/K_r = a(1 + bc_\mathrm{t}) = ab[c_\mathrm{t} + (1/b)] \quad (3)$$

It seems proper, however, to include the factor c_mt (total active site concentration) only in the coefficient a, since c_mt is most likely to be affected by the state of activation of a particular catalyst. Thus a is an inverse measure of the relative activity of a catalyst. On this basis there are two linear reduced forms appearing as Eqs. (3) and (4) in Table 1. The two-site mechanisms lead to square-root terms, as shown in Eqs. (5) and (6).

Eight of the ten kinetic schemes (including the second Rideal mechanism) lead to expressions of the same form as Eq. (2), which represents the published data. Other mechanisms can doubtless be postulated which would lead to rate expressions of the kinetic form found experimentally. It seems evident that kinetic data alone cannot resolve the question of mechanism of the conversion, though perhaps one or more of the postulates can be eliminated.

Pore diffusion. A meaningful kinetic analysis must focus on the specific rate coefficient K_r rather than on the overall rate coefficient K_0 derived from experimental data. For this purpose it is necessary to estimate the importance of mass transfer from bulk gas to the porous catalyst, and of diffusion within the porous structure.

Following Thiele (*23*), an effectiveness factor η is defined as the reaction rate within the porous structure as a fraction of the rate which would obtain if all the internal surface were exposed to the reactant concentration c_ps which is maintained in the gas immediately adjacent to the pellet surface. Equation (1) is then rewritten

$$r = \eta WK_r(c_\mathrm{ps} - c_\mathrm{pe}) \quad (7)$$

The porous pellets employed in the studies to be described were formed by pressing powders into noncatalytic steel rings. For this "slab" geometry and isothermal first order reaction and diffusion, η is given by

$$\eta = \tanh \phi/\phi; \qquad \phi \equiv [K_r\rho_\mathrm{p}L^2/D_\mathrm{eff}]^{1/2} \quad (8)$$

where L is half the slab thickness (half the cylinder height), ρ_p is the pellet density, and D_eff is the effective diffusion coefficient based on superficial pellet area.

At large values of ϕ, η approaches $1/\phi$.

For this region of low effectiveness, Eqs. (3), (7), and (8) may be combined to give

$$r = \frac{W}{L}\left[\frac{D_{\text{eff}}}{a\rho_p}\right]^{1/2} \frac{(c_{ps} - c_{pc})}{(1 + bc_t)^{1/2}} \qquad (9)$$

Diffusion within the pores may be by bulk or molecular diffusion, with D_{eff} inversely proportional to P, or by Knudsen diffusion, independent of P, or simultaneously by both mechanisms. Thus total pressure may enter Eq. (9) through both D_{eff} and c_t.

Several authors have reported studies of the conversion in cases where pore diffusion is important. Wicke and Brötz (*25*) found a pressure effect on η through its effect on the bulk diffusivity in the large "pores" of a tube packed with nickel chips. Smith and co-workers (*16–18*) investigated the effects of varying pellet density (and therefore pore sizes and distributions) on effectiveness. Others (*13, 14, 24*) have reported a particle-size effect, i.e., the effect of L on η [Eq. (8)]. The present study of pore diffusion differs in concentrating on the effects of varying the reaction rate coefficient, both by switching catalyst samples and by varying pressure.

Mass transfer from gas to catalyst. Equation (9) relates the reaction rate to the pellet surface concentration, c_{ps}. Since it is the ambient gas concentration c_p that is measured, it is desirable to formulate a relation in which c_{ps} is eliminated, or to relate K_r to K_0. For the steady state condition, the rate of mass transfer from gas to pellet may be equated to the rate of chemical conversion

$$r = WK_0(c_p - c_{pc}) = \eta WK_r(c_{ps} - c_{pc}) = k_c A_p(c_p - c_{ps}) \qquad (10)$$

whence

$$\frac{1}{WK_0} = \frac{1}{\eta WK_r} + \frac{1}{k_c A_p} \qquad (11)$$

where $(WK_0)^{-1}$ may be called the "overall reaction resistance."

Methods of estimating the mass-transfer coefficient k_c are reviewed by Satterfield and Sherwood (*21*) and by numerous other texts. At low gas flow rates k_c for transfer from gas to a sphere of diameter d_p is given by

$$K_c = 2\frac{D_B}{d_p} \qquad (12)$$

which is a good approximation for $N_{Re}N_{Sc}^{2/3} < 1$. The effect of total pressure enters through k_c, since the molecular diffusion coefficient D_B is inversely proportional to pressure. For the hydrogen system D_B is 1.442 cm²/sec at 20°C and 1.0 atm (*10*).

Graphical representation of rate equations. The interpretation of experimental data on catalytic conversion is facilitated by employing methods of plotting which distinguish the basic kinetics from the effects of mass transfer and pore diffusion. Several methods applicable to data on hydrogen conversion are illustrated by Fig. 1; these are based on the corresponding equations and conditions given in Table 2, which in turn are the results of combining Eqs. (9) and (11) with (3) or (4).

As noted earlier, a is assumed to be inversely proportional to c_{mt}, and an inverse measure of catalyst activity. It is assumed that catalyst activation procedures or a change in reaction temperature affect only the quantity a. The illustrations are limited to those cases where η is either unity or very small and inversely proportional to ϕ. Pore diffusion is taken to be independent of pressure, as in the case of Knudsen diffusion. As a reminder of the effect of pressure on external or bulk mass transfer, k_c is replaced by k_c'/c_t, where k_c' is independent of P and c_t proportional to P.

Experimental Methods

The conversion was carried out in a continuous-flow system, with catalyst supported near the center of an unstirred 200-ml glass reaction vessel. In all tests the feed gas was 50.2% p-H_2, and the equilibrium composition at reaction temperature was 25.0% p-H_2.

Figure 2 is a diagram of the flow system. Prepurified hydrogen entered through a vacuum pressure regulator (Matheson), Deoxo and Drierite cylinders, and then split into reference and sample streams. The two streams were compared in a thermal-conductivity cell (Gow-Mac JDC-301) maintained at 0°C, followed by pressure and flow-rate measurement using absolute mercury manometers and capillary flow meters. Each stream then passed through a vacuum

TABLE 1

REACTION MECHANISMS AND KINETIC EQUATIONS FROM STEADY STATE ANALYSIS

Mechanisms[a]		Reduced form of reaction rate equation, where $r/W = K_r(c_p - c_{pe})$ and
Bonhoeffer-Farkas Type	Rideal-Eley Type	
1. Single-site, or Schwab (*22*)	7. Second Rideal (*19*)	
$p(g) + M \rightleftarrows {}^{p}M$	$p(g) + MM \rightleftarrows {}^{H\ Hp}MM$	
$o(g) + M \rightleftarrows {}^{o}M$	$o(g) + MM \rightleftarrows {}^{H\ Ho}MM$	$1/K_r = a(1 + bc_t)$ (3)[b]
$M \rightleftarrows {}^{p\ o}M$	$MM \rightleftarrows {}^{Hp\ Ho}MM$	
2. Type 1, coupled with nonspecific molecular adsorption	8. Boreskov and Vassilevitch (*3*)	
$p(g) \rightleftarrows p(s)$	$p(g) \rightleftarrows p(s)$	
$o(g) \rightleftarrows o(s)$	$o(g) \rightleftarrows o(s)$	
$p(s) + M \rightleftarrows {}^{p}M$	$p(s) + MM \rightleftarrows {}^{H\ Hp}MM$	$1/K_r = a(1 + b_1c_t) + b_2$ (4)[b]
$o(s) + M \rightleftarrows {}^{o}M$	$o(s) + MM \rightleftarrows {}^{H\ Ho}MM$	
$M \rightleftarrows {}^{p\ o}M$	$MM \rightleftarrows {}^{Hp\ Ho}MM$	
3. Single-site, with o and p indistinguishable on surface	9. First Rideal (*19*)	
$p(g) + M \rightleftarrows {}^{H_2}M \rightleftarrows M + o(g)$	$p(g) + M \rightleftarrows {}^{H\ H_2\ H}M \rightleftarrows M + o(g)$	$1/K_r = a(1 + bc_t)$ (3)
4. Type 3, coupled with nonspecific molecular adsorption	10. Eley (*5*), or Bond (*1*)	
$p(g) \rightleftarrows p(s)$	$p(g) \rightleftarrows p(s)$	
$o(g) \rightleftarrows o(s)$	$o(g) \rightleftarrows o(s)$	$1/K_r = a(1 + b_1c_t) + b_2$ (4)
$p(s) + M \rightleftarrows {}^{H_2}M \rightleftarrows M + o(s)$	$p(s) + M \rightleftarrows {}^{H\ H_3\ H}M \rightleftarrows M + o(s)$	

5. Two-site, original Bonhoeffer-Farkas (*2*) $\mathrm{p(g) + MM \rightleftarrows \overset{H}{M}\overset{H}{M} \rightleftarrows MM + o(g)}$	None	$1/K_r = a^2[1 + (bc_t)^{1/2}]^2$ (5)
6. Type 5, coupled with nonspecific molecular adsorption $\mathrm{p(g) \rightleftarrows p(s)}$ $\mathrm{o(g) \rightleftarrows o(s)}$ $\mathrm{p(s) + MM \rightleftarrows \overset{H}{M}\overset{H}{M} \rightleftarrows MM + o(s)}$	None	$1/K_r = a^2[1 + (b_1c_t)^{1/2}]^2 + b_2$ (6)

[a] Notation: M = adsorption site; p, o = p-H_2, o-H_2; (g) = gas, (s) = surface.
[b] Derived in Appendix.

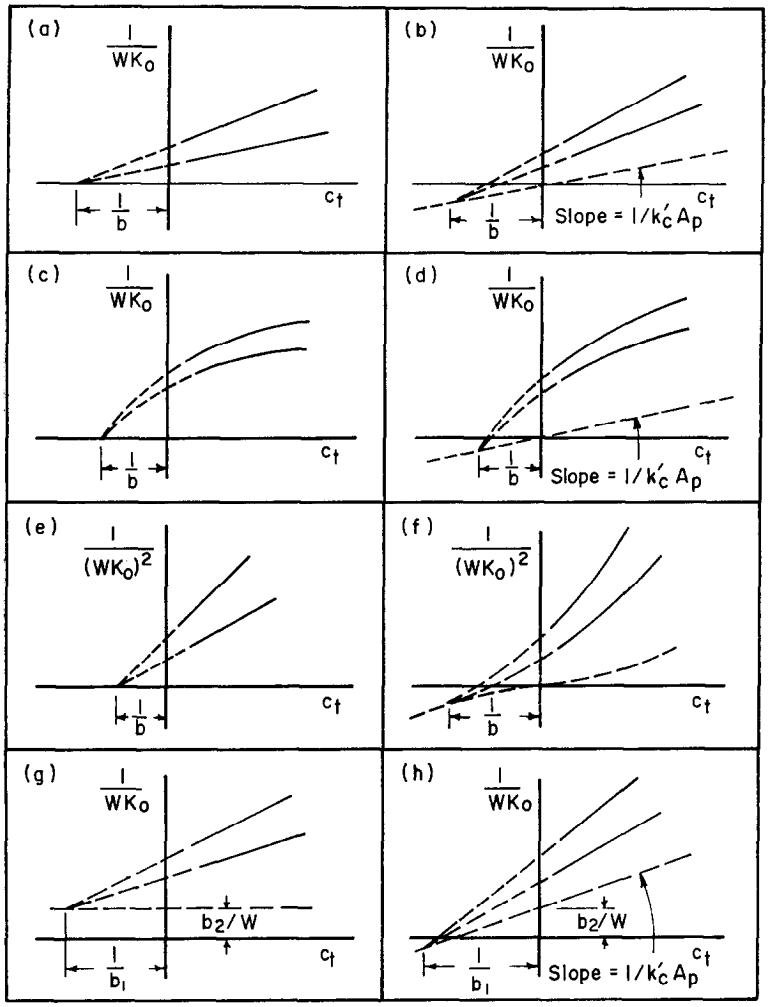

FIG. 1. Methods of plotting experimental data for interpretation of kinetics. See Table 2. In each case the upper curve is for the less active catalyst.

needle valve (Hoke) to a vacuum pump. Series of tests were made at 80 to 740 mm Hg and 0.3 to 1.7 cm^3/sec (at reactor conditions). Copper tubing, brazed joints, and Hoke bellows vacuum valves were employed to ensure vacuum tightness. The low-temperature glass converter and glass reaction vessel were connected to the metal tubing by Kovar-glass seals. A high-vacuum line, connected to the reactor by an NRC block valve, was used for leak-testing and for catalyst activation.

A Gow-Mac DC power supply delivered 200 mA to the conductivity cell, providing a low-noise signal of adequate magnitude (0 to 4 mV for 25 to 50% p-H_2) without overloading the cooling bath. Immersion of the two 100-ohm bridge resistors in a flask of mineral oil reduced electrical drift and noise. Pressure and flow rate had little effect on the cell signal. Fluctuations in cell signal due to variations in cell temperature were minimized by frequent replenishment of ice in the Dewar and by the use of a small air stream to stir the ice-water mixture.

The 50.2 mole % p-H_2 feed was prepared by passing the purified normal hydrogen at low flow rates through a large excess of NiO/alumina catalyst maintained at liquid nitrogen temperature. Reactor effluent com-

TABLE 2
EQUATIONS ON WHICH THE METHODS OF PLOTTING EXPERIMENTAL DATA ARE BASED

Figure	Reaction kinetics equation	η	BMTR[a]	Equation
1a	(3)	1	No	$\frac{1}{WK_0} = \frac{a}{W}(1 + bc_t)$
1b	(3)	1	Yes	$\frac{1}{WK_0} = \frac{a}{W}(1 + bc_t) + \frac{c_t}{k_c' A_p}$
1c	(3)	$\ll 1$	No	$\frac{1}{WK_0} = \frac{L}{W}\left(\frac{a\rho_p}{D_{eff}}\right)^{1/2}(1 + bc_t)^{1/2}$
1d	(3)	$\ll 1$	Yes	$\frac{1}{WK_0} = \frac{L}{W}\left(\frac{a\rho_p}{D_{eff}}\right)^{1/2}(1 + bc_t)^{1/2} + \frac{c_t}{k_c' A_p}$
1e	(3)	$\ll 1$	No	$\left(\frac{1}{WK_0}\right)^2 = \frac{L^2}{W^2}\left(\frac{a\rho_p}{D_{eff}}\right)(1 + bc_t)$
1f	(3)	$\ll 1$	Yes	$\left(\frac{1}{WK_0}\right)^2 = \left[\frac{L}{W}\left(\frac{a\rho_p}{D_{eff}}\right)^{1/2}(1 + bc_t)^{1/2} + \frac{c_t}{k_c' A_p}\right]^2$
1g	(4)	1	No	$\frac{1}{WK_0} = \frac{a}{W}(1 + b_1 c_t) + \frac{b_2}{W}$
1h	(4)	1	Yes	$\frac{1}{WK_0} = \frac{a}{W}(1 + b_1 c_t) + \frac{b_2}{W} + \frac{c_t}{k_c' A_p}$

[a] Refers to presence or absence of a bulk mass-transfer resistance (between gas and catalyst).

position was measured by comparing consecutive signals from normal hydrogen, reactor feed, and reactor effluent with the normal hydrogen reference. Minor corrections were made to "zero" all measurements so that normal hydrogen from all three lines gave the same adjusted signal.

The reactor was a 200-ml round unstirred Pyrex vessel. Catalyst—supported on a glass platform at the center of the vessel—was installed and removed through short tubing opened and sealed each time. Powder catalyst was spread on a 15-mm diameter glass dish; pelleted catalyst (in a steel ring) rested directly on the same platform. Reactor gas temperature was found to be within ± 0.1°C of the water-bath temperature at 25° to 65°C. No conversion was measurable when the reactor containing a steel pellet ring was operated without catalyst. Gas compositions, calculated from the continuously recorded cell signals, were believed accurate to $\pm 0.02\%$ p-H_2.

Catalyst samples were prepared from powdered Girdler T-310 NiO/alumina pellets. Catalyst for Series P-9 was a 74–104 μ screened fraction of this material; all other tests were made with catalyst (both powder and pellets) prepared from a 44–62 μ fraction. Pellets were formed and retained in steel rings 3.15 mm high with two faces 4.75 mm in diameter. The open faces were sanded down to be flush with the rings, but density gradients doubtless existed in the cylindrical pellet, as noted by Satterfield and Saraf in a study made with pellets made in a similar way (*20*). Physical measurements on the catalyst are given in Table 3.

Catalyst activation, a combination of vacuum pumping, heating, and hydrogen purging at 300 mm, varied from sample to sample. In almost all cases the evacuation and pumping steps (both with the outside of the reactor maintained at 250–300°C) were several hours each. Initially it was postulated that the lower the vacuum pressure (in the 10^{-5}-mm region) the more active would be the catalyst, but no such correlation was observed. Furthermore, it was concluded after a few tests that reevacuation

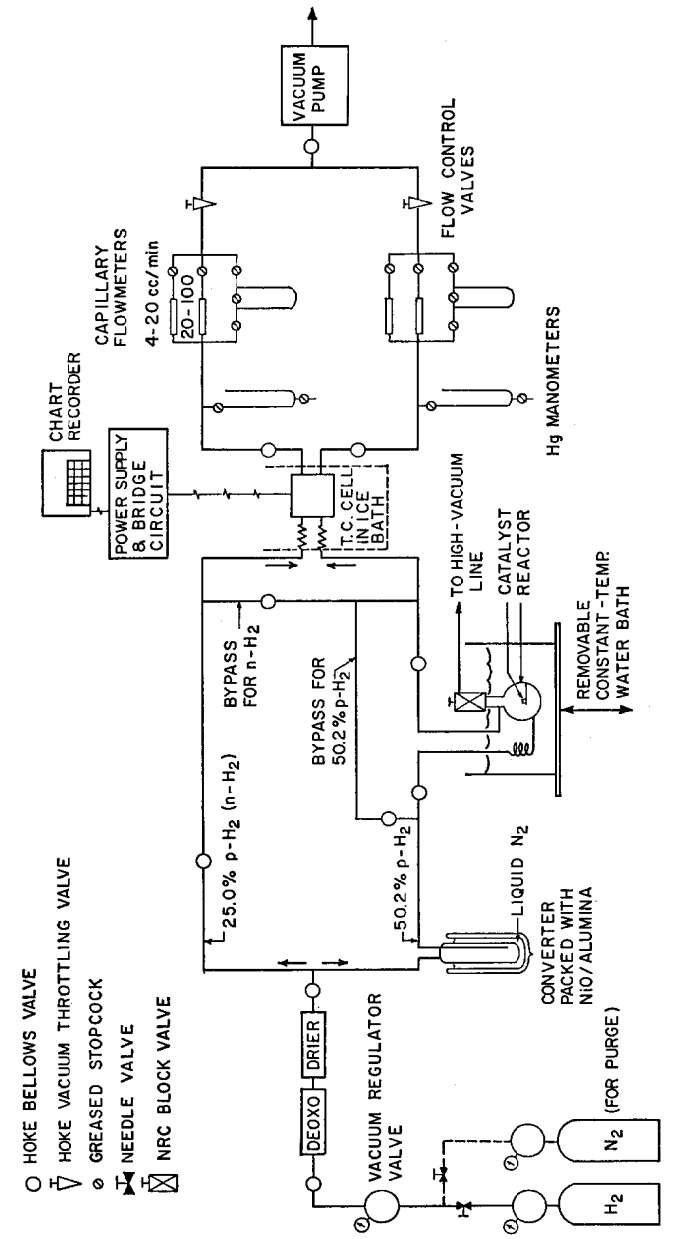

FIG. 2. Flow diagram of experimental reaction system.

TABLE 3
CATALYST PROPERTIES

A. Manufacturer's Data, original Girdler T-310 pellets before crushing: 10–12 wt % NiO on alumina, 3/16 × 1/8 inch, 220 m^2/g (BET), pore volume (CCl_4 absorption) 0.32 cm^3/g at 800 Å, 0.27 cm^3/g at 140 Å

B. Measurements on pellet sample (courtesy Union Oil Co. of Calif.): 10 cm^3 8–60 mesh broken pellets made as tested in "low-density" pellet runs, from 44–62 μ powder in steel rings; calculated density 1.58 g/cm^3[a]

Measured	
Surface area (BET), m^2/g	131
Pellet Density (Hg immersion), g/cm^3	1.47[a]
Solid volume (He displacement), cm^3/g	0.29
Calculated from Above	
Pore volume, cm^3/g	0.39
Av. pore diameter, Å	119
Porosity	0.57

[a] Discrepancy not explained—possibly due to insufficient penetration by mercury in immersion test.

following hydrogen purging resulted in a less active catalyst. Exceptionally high or low activities of certain powder catalysts were associated with special activation effects; these are discussed below.

Experiments were made with powdered catalyst and with both "low-density" (1.57–1.61 g/cm^3) and "high-density" (1.76–1.81 g/cm^3) pelleted catalyst. Catalyst samples were reactivated or replaced after each series of tests. Within each series the sequence of pressure and temperature settings was sufficiently random to establish that the results were independent of the order of the tests. Measurements were made of reactor temperature and pressure, flow rate, and conductivity-cell signals in each test. The feed was assumed to be 50.2% p-H_2, whence

$$\frac{1}{WK_0} = \frac{y_p - 0.250}{Q(0.502 - y_p)} \qquad (13)$$

where y_p is the mole fraction p-H_2 in the effluent and Q is the volumetric flow rate (cm^3/sec) at the measured temperature and pressure. The implied assumption that the ambient and effluent concentrations were the same is discussed below.

RESULTS

Gas mixing in reactor. Values of K_0 were calculated from the conversion data by the use of Eq. (13), with y_p taken as equal to the measured p-H_2 mole fraction in the reactor effluent. This procedure was justified by experimental "wash-out" tests, which showed the reactor to be well mixed at the pressures and flow rates employed in the kinetic study. The effluent composition was monitored following a sudden change in feed composition from normal hydrogen to 50.2% p-hydrogen; it followed closely the exponential decay typical of well-stirred reactors, at both high and low flow rates and pressures. In other tests it was found that the operation of a small magnetic stirrer within the reactor caused no observable effect on effluent gas composition during either "wash-out" or conversion tests.

Equatiun (13) can be rewritten as

$$\frac{1}{0.502 - y_p} = 3.97\left(1 + \frac{Q}{WK_0}\right) \qquad (14)$$

From this it follows that $(0.502 - y_p)^{-1}$ should be linear in Q if the reactor is well stirred and if K_0 is independent of Q. Conversion tests with both pellets and powder showed this to be true; graphs of $(0.502 - y_p)^{-1}$ vs. Q at constant pressure gave excellent straight lines in nearly all cases, lines for different pressures converging to the common intercept of 3.97. Exceptions were noted in a few cases at the lowest

pressure, when the intercept was 4.1–4.2. Incomplete mixing of the gases in the reactor or small air leaks at the lowest pressures would cause deviations in the opposite direction; it is suspected that these discrepancies were due to reconversion to p-H_2 in the copper tubing between converter and reactor, significant only at low pressures and flow rates.

Thus it was concluded that the reactor could be considered to be well-stirred. The uniformity of the gas concentration within the reactor was the consequence of the rapid molecular diffusion in a hydrogen system, and the relatively long residence times of 3 to 10 min.

Mass transfer to catalyst. The resistance to mass transfer, gas to catalyst surface, was evidently a small fraction of the total in most tests. This is most strongly suggested by the fact that different catalyst activation procedures led to 100-fold changes in conversion rates under similar test conditions. Furthermore, the straight lines obtained on graphs of $(0.502 - y_p)^{-1}$ vs. Q at constant pressure showed K_0 to be independent of gas flow rate.

Estimation of k_c by Eq. (12) and substitution in Eq. (11) suggested that the resistance $(k_c A_p)^{-1}$ was typically less than 10% of the total resistance $(WK_0)^{-1}$. In the extreme case of the most active catalyst, however, the bulk-gas mass-transfer resistance may have been as much as half the total.

Kinetic data. The conversion data obtained with powder catalyst and low- and high-density pellets are plotted as $(WK_0)^{-1}$ or $(WK_0)^{-2}$ vs. $c_t(= P/RT)$ on Figs. 3, 6–8, and as log K_0 vs. $1/T$ on Figs. 4 and 9. Each series of tests involved measurements over a range of pressures at constant temperature, or measurements at constant pressure over a range of temperatures. Flow rates, which varied from 0.3 to 1.7 cm³/sec, are not shown on the figures, since flow rate did not affect the results. Calculated values of K_0 and activation energies are shown in Table 4. The values of K_0 tabulated are interpolated for the common condition of P = 715 mm, T = 28.8°C.

The external catalyst surface A_p varied little with W; in the case of the pellets A_p was essentially the same in each test though W varied between series. The variable $(WK_0)^{-1}$ is employed instead of K_0^{-1} for this reason, since the mass-transfer term in Eq. (11) is then dependent only on pressure and temperature. Apparent activation energies were calculated from the slopes of the Arrhenius graphs shown as Figs. 4 and 9, all data being obtained at 704 to 734 mm Hg.

TABLE 4
SUMMARY OF RESULTS[a]

Series	W (g)	K_0[b] (cm³/sec-g)	E, apparent (kcal/mole)	η (= $K_0/260$)
		Powder Catalyst		
P-3	0.0172	260	—	
P-4A	0.0058	25	9.34	
P-4B	0.0058	10	8.87	
P-4C	0.0058	4.9	10.38	
P-5	0.0096	260	—	
P-6	0.0082	290	—	
P-7	0.0057	320	—	
P-8	0.0040	260	—	
P-9	0.0052	260	3.48	
P-10A	0.0054	640	1.63	
P-10B[c]	0.0054	15	—	
P-10C[c]	0.0054	103	—	
P-10D[c]	0.0054	62	—	
		Low-Density Pellets		
LDP-2	0.0909	15	—	0.058
LDP-3	0.0904	8.9	2.86	0.034
LDP-4A	0.0855	10.5	2.76	0.040
LDP-4B	0.0855	13.1	2.31	0.050
LDP-6	0.0861	20	2.62	0.077
		High-Density Pellets		
HDP-5A	0.1002	14.5	1.33	0.056
HDP-5C	0.1002	15.5	2.50	0.060
HDP-7A	0.0944	7.6	—	0.029
HDP-7B	0.0944	10.2	2.90	0.039

[a] All series with pressure varied were at 28.8°C and 80–740 mm Hg except HDP-7A (three isothermal runs at 28.9°, 58.3°, and 44.1°C) and HDP-7B (two isothermal runs at 28.9° and 58.2°C). All series with temperature varied were at a pressure between 704 and 734 mm Hg and 25–65°C except HDP-7B in which one point was taken at 4°C.

[b] Est. for 715 mm, 28.8°C.

[c] Series 10-B, 10-C, and 10-D showed an initial drift of activity (K_0) and are not plotted.

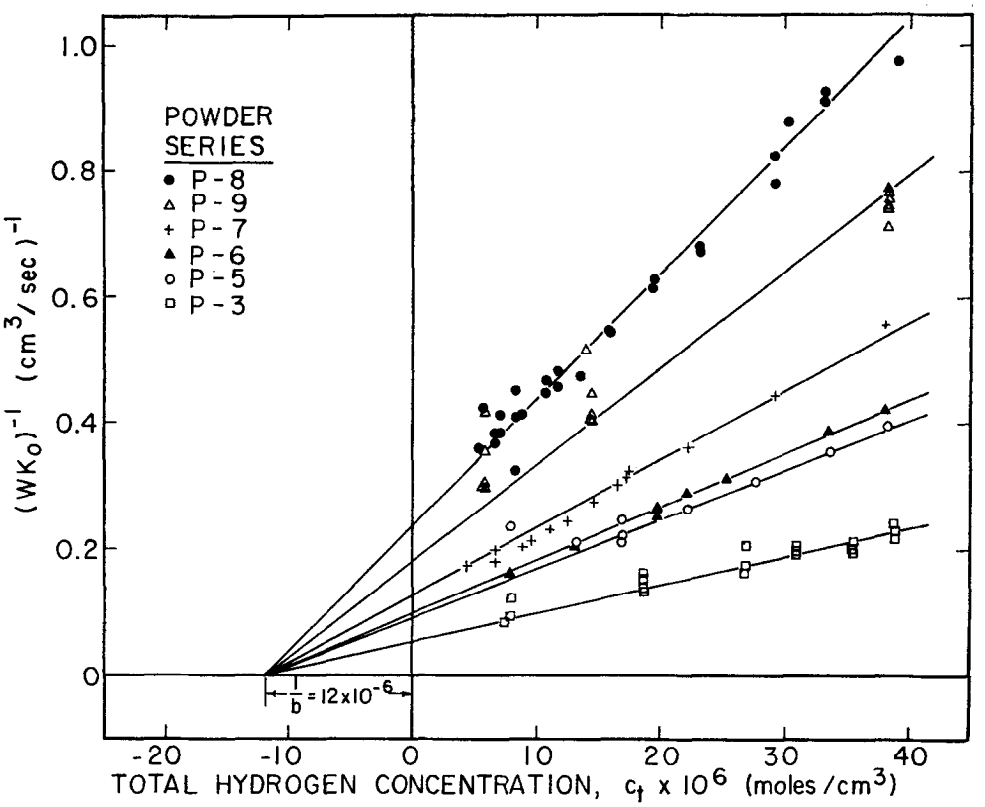

FIG. 3. Powder catalysts, isothermal kinetic data. $T = 28.8°C$ for all series. Best straight lines fit to give common intersection.

DISCUSSION

Powder Catalyst. The isothermal powder data, shown on Fig. 3, are seen to conform to the linear Eqs. (2) and (3). The observed effect of pressure agrees with the results of several previous investigators. Though the straight lines shown were forced slightly to converge to a common intercept on the c_t axis, it is evident that b is approximately the same for the various tests. The different activation procedures employed did not change b, but caused a to vary several fold [a is proportional to the intercepts with the $(WK_0)^{-1}$ axis].

The conclusion that bulk mass-transfer resistances were small is supported by the common intersection on the c_t axis; the pattern is that of case 1a rather than 1b of Fig. 1 and Table 2. The small powder samples had low bulk densities and high porosity (being spread as a thin layer on the support dish), so the effectiveness factor in these tests was essentially unity. It can be concluded that the overall coefficient K_0 is equal to the reaction coefficient K_r and that the powder data depend on the intrinsic kinetics of the surface reaction.

The correlation of the powder data shown as Fig. 3 supports Mechanisms 1, 7, 3, and 9 of Table 1, but not Mechanisms 2, 4, 5, 6, 8, or 10. However, if in Mechanisms 2, 4, 8, and 10 it be assumed that molecular desorption is very rapid compared with surface conversion, the constant b_2 of Eq. (4) drops out. The kinetic data cannot differentiate among eight of the mechanisms; only the two-site mechanisms (5) and (6) are ruled out. However, the data support the two-step mechanisms involving nonspecific outer-layer molecular adsorption only if very rapid

molecular desorption is postulated. This is not an objectionable assumption, but would be questionable if applied to more strongly bonded "inner-layer" species.

Figure 4 is an Arrhenius graph of powder data obtained over a small temperature range. The activity varied widely from one series to another, due in part to different activation procedures and due also to catalyst poisoning on certain occasions when the catalyst was exposed to the untrapped vacuum pumps overnight (prior to series P-4B and P-4C). These changes in activity showed a compensation effect, as illustrated by Fig. 5. Of all the powder tests, series P-9 is the most comparable to the pellet tests because of similar activation histories. The very high activity (K_0 = 640) for series

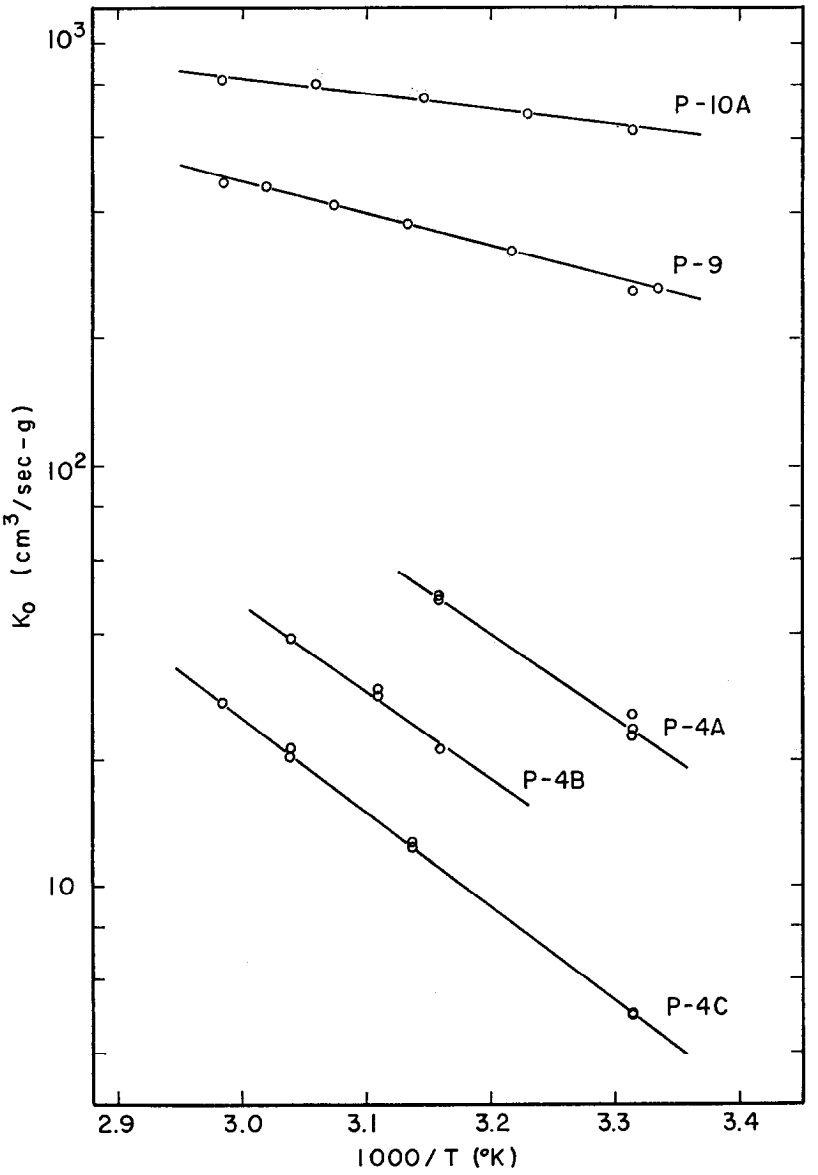

FIG. 4. Powder catalysts, Arrhenius plot. All data for P = 706 to 726 mm.

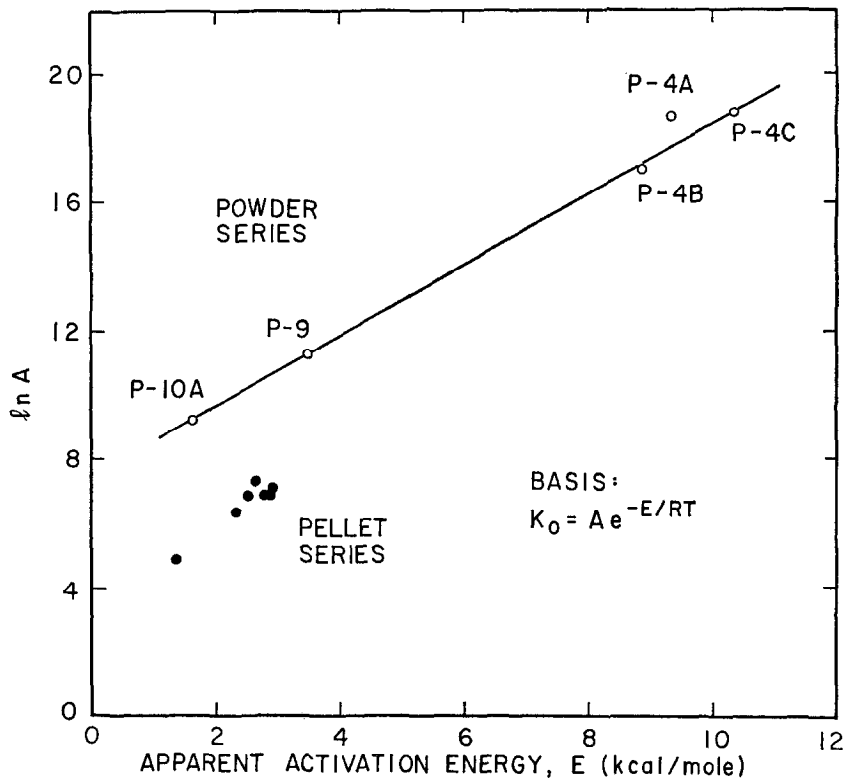

FIG. 5. Compensation effect for powder catalysts. Data from Fig. 4. Pellet data from Fig. 9 also shown.

P-10A is probably the result of the unique activation procedure employed. This involved a single long hydrogen purge with heating after evacuation, rather than the customary two short purges and overnight sealing in hydrogen.

Compensation effects for the hydrogen conversion on metals have been reported elsewhere (*7, 8, 11, 12*). Holden and Rossington (*11*) even found that independent conversion data for the same metal, and in some cases different metals, could be correlated by the same compensation effect. This supported the suggestion of Couper and Eley (*6*) that it is better to speak of a characteristic E — log A relation than a characteristic E for a given metal. Several explanations for the effect have been reviewed by Cremer (*7*). A simple qualitative argument may be provisionally cited for the present case where it is fairly certain that the high-E catalysts were subjected to the poisoning effect of diffusion-pump oil. That is, the net activity of the unpoisoned catalysts is dominated by a small number (low A) of very active (low E) sites. The poison tends to block these sites, resulting in a net activity dominated by a larger number (higher A) of less active (higher E) sites.

The apparent activation energies given in Table 4 involve contributions from the several sequential steps of any reaction mechanism. These values can be corrected for the temperature dependence of gas-to-catalyst mass transfer and of gas concentration at constant pressure to obtain the true activation energy of the overall surface reaction. If it be assumed the mass transfer presented 10% of the total resistance in the powder runs, then the true activation energies are within 0.5 kcal of the apparent values given in Table 4.

Pelleted catalysts. As may be seen from Table 4, the values of K_0 for pellets were much smaller than for the active powders. This is to be expected, because of the large resistance to diffusion within the porous catalyst structure. Assuming a K_0 of

260 (Series P-5, P-6, P-8, and P-9) to be representative of unpoisoned catalyst with no mass-transfer resistance, the pellet effectiveness factors may be estimated as simply $K_0/260$. These approximate values of η are given in Table 4.

The data obtained with the high-density pellets are shown in Fig. 6, on which $(WK_0)^{-2}$ is plotted vs. c_t. The straight lines and common intercept on the c_t axis conform to the kinetics exhibited by the powders, modified to allow for pore diffusion with a low effectiveness factor [see Fig. 1(e) and Table 2]. The intercept $1/b$ is now 2×10^{-6}, whereas it was found to be 12×10^{-6} for the powders (Fig. 3). The "adsorption coefficient" b involves the ratio of the adsorption to desorption rate coefficients and is a measure of the strength of adsorption. Possibly the greater concentration of surface forces in a porous compressed mass leads to greater hydrogen adsorption at a given hydrogen

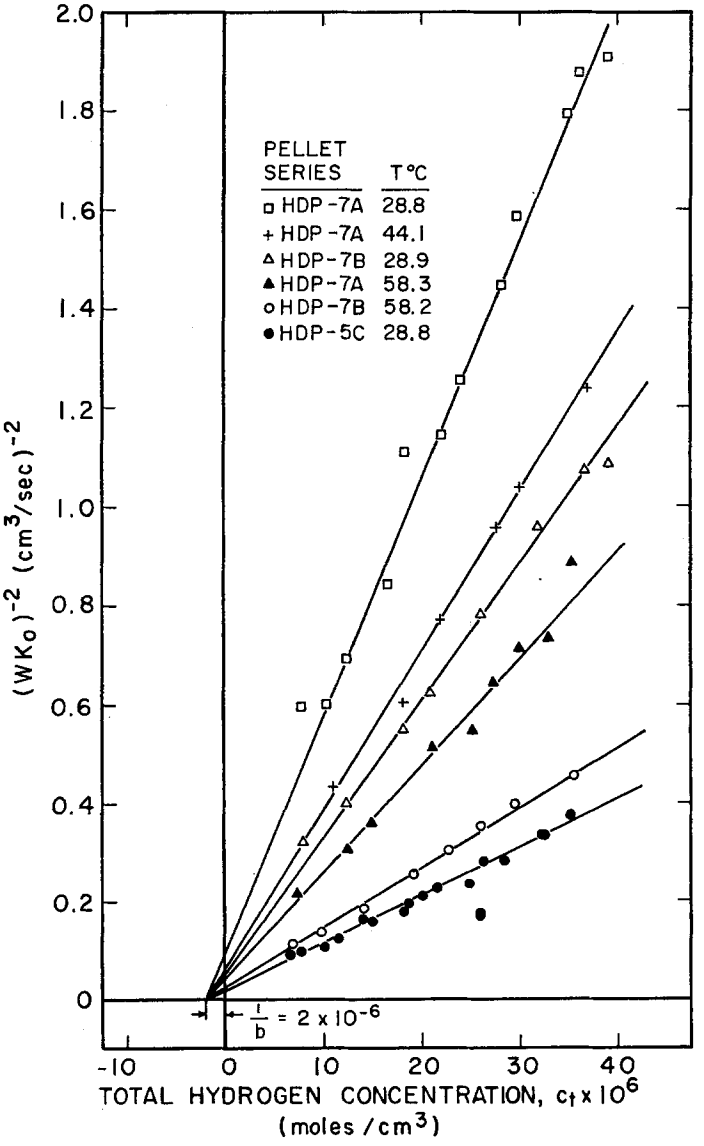

FIG. 6. High-density pellets, isothermal kinetic data. Best straight-line fits.

pressure. It is difficult, however, to explain the sixfold difference.

The data on the low-density pellets, shown in Figs. 7 and 8, exhibit certain anomalies which are difficult to explain. Comparison of Fig. 7 with Fig. 3, and of Fig. 8 with Fig. 6, shows that these results fit the pattern of the powder data much better than that of the data on the high-density pellets. There is a greater possibility of loose powder falling away from the pressed faces of the low-density pellets and so giving powderlike behavior (some powder was observed in the reactor during series LDP-2), but if this were significant K_0 would have been much larger than in the high-density pellet tests.

It is conceivable that Knudsen diffusion prevailed in the high-density pellets and ordinary molecular diffusion in the larger pores of the low-density pellets. Since the latter is inversely proportional to pressure (and to c_t) the concave-upwards relation shown by Fig. 8 might be explained.

The apparent activation energies and the overall rate coefficients (Table 4, Fig. 9) are roughly the same for both low- and high-density pellets, but somewhat lower than for the powder run P9. It is well known

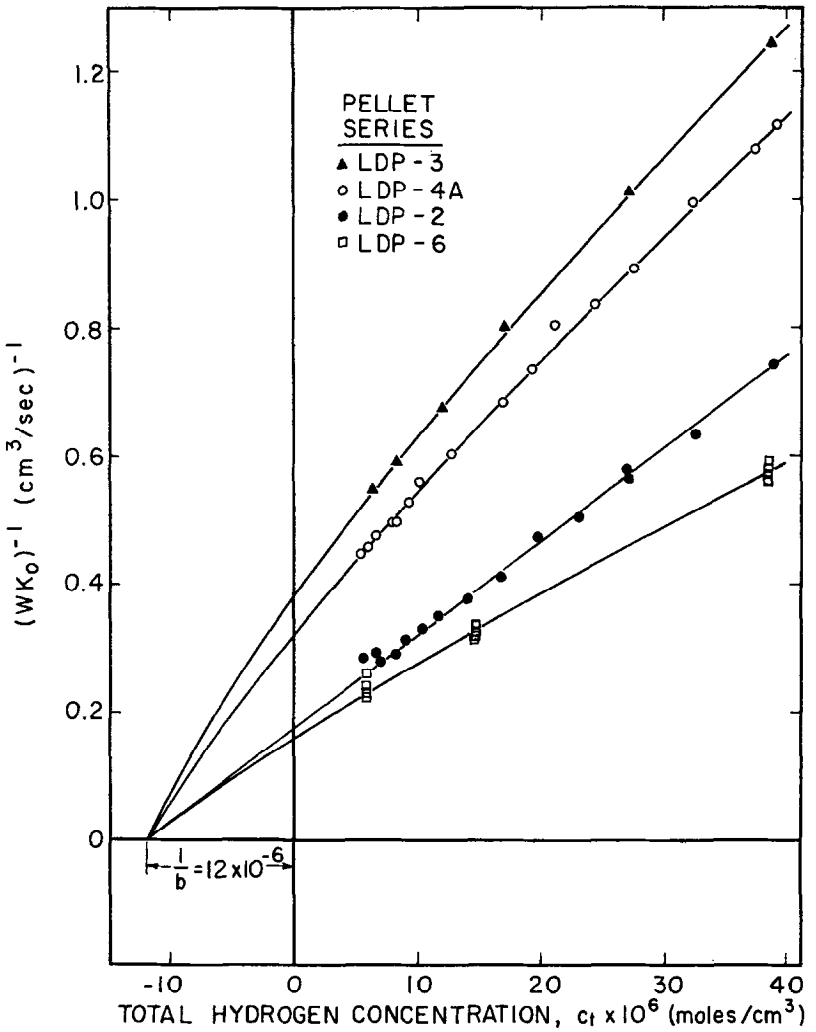

FIG. 7. Low-density pellets, isothermal kinetic data plotted as first power of overall resistance. T = 28.8°C for all series. Intersection forced to be same as Fig. 3.

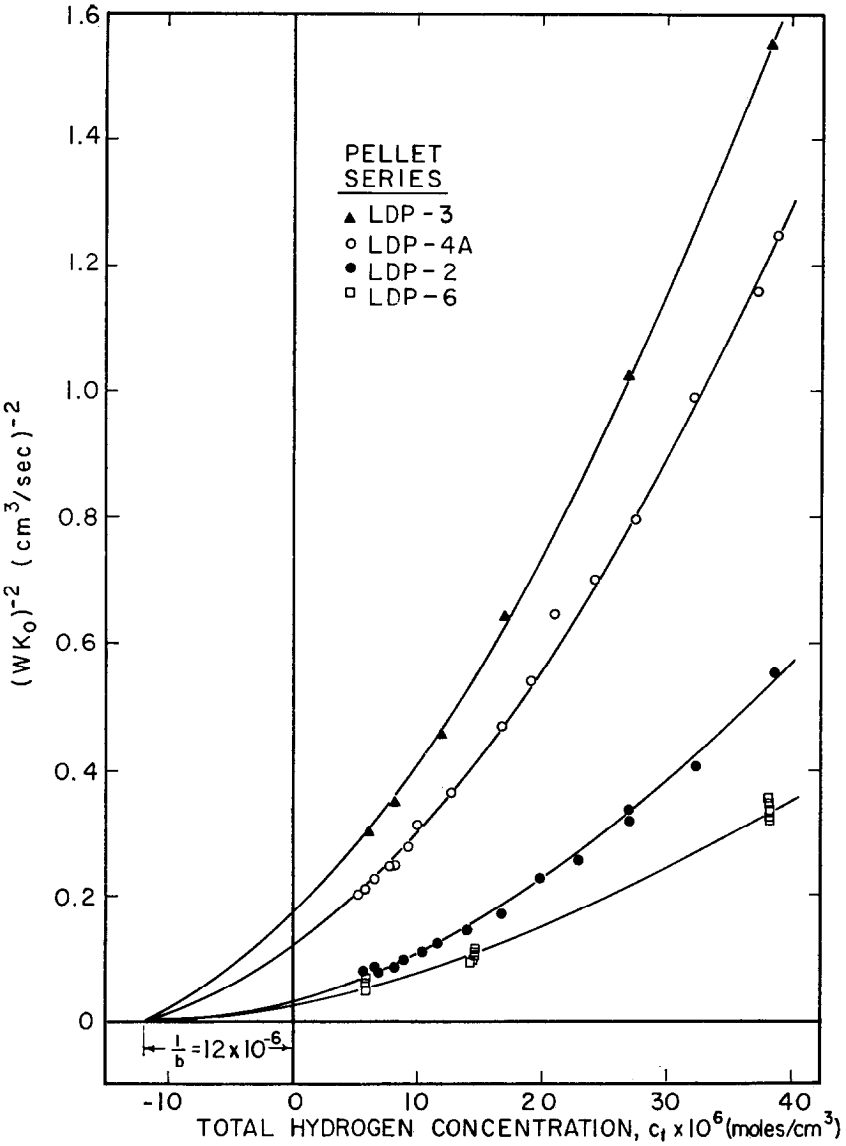

FIG. 8. Low-density pellets, isothermal kinetic data plotted as second power of overall resistance. T = 28.8°C for all series. Intersection forced to be same as Fig. 3.

that pore-diffusion resistance reduces the apparent activation energy of the overall process: It is approximately halved when the effectiveness factor is small. The true activation energy for both types of pellets, after correcting for pore diffusion and mass transfer, appears to be 4.5–5.0 kcal/mole.

The effectiveness factors for the pellets could be calculated using Eq. (8) and the catalyst data given in Table 3 (along with intrinsic rate coefficients estimated from the data) if D_{eff} were known [see ref. (*21*)]. Alternatively, the observed values can be employed to calculate D_{eff}. Lacking data on catalyst pore-size distributions, a simple uniform-pore model is used and the "tortuosity" factor τ may be calculated for comparison with previous data. At 720 mm and 28.8°C the molecular diffusion coefficient is 1.59 cm^2/sec; for 119-Å pores the Knudsen coefficient is 0.0715 cm^2/sec, whence D_{eff} for a porosity of 0.57 is $0.041/\tau$ cm^2/sec. In

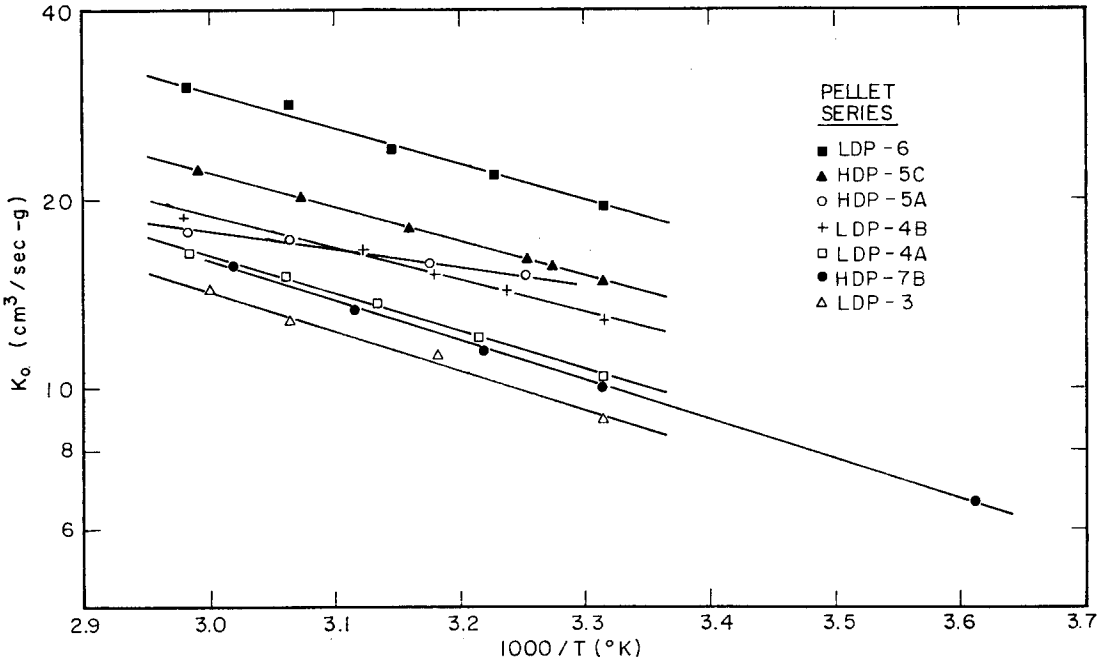

FIG. 9. High- and low-density pellets, Arrhenius plot. All data for P = 723 to 733 mm.

the range of low effectiveness factors of interest η is inversely proportional to ϕ; with K_r = 260 cm³/(sec)(g), τ is found to be $43 \times 10^{-4}/\eta^2$. The data used are for the low-density pellets (corresponding to the sample in Table 3); these gave values of η ranging from 0.034 to 0.077. The corresponding values of τ are 0.7–3.7. This is the range of values of τ reported for similar porous materials (*21*).

Although the catalyst physical data do not justify further refinement of these calculations, it is worth noting that τ, as calculated, is proportional to the product $d_e K_r$. Thus, for example, if d_e were doubled to reflect the expected dominance of macropores in the diffusion process, and K_r were halved under the assumption that the intrinsic activity of the pellet catalysts was less than the typical activity of the powder catalysts, τ would be unchanged. In this example η would be doubled but would still be low enough for Eq. (9) to apply.

SUMMARY

Conversion of para- to orthohydrogen at 100–740 mm Hg total pressure at near room temperature, using powdered nickel/alumina catalyst, was found to follow the rate equation

$$r = W(c_p - c_e)/a(1 + bc_t)$$

This result, in agreement with the work of other investigators, is compatible with several variations of both the Bonhoeffer-Farkas and Rideal-Eley mechanisms.

The rate of conversion using high-density pellets of the same catalyst is given by

$$r \propto (c_p - c_e)/(1 + bc_t)^{1/2}$$

This form is exactly predicted by the pore-diffusion theory, using the same intrinsic reaction kinetics as for the powder catalyst. It holds for pellets with low effectiveness factors and negligible resistance to mass transfer between gas and catalyst. Deviation of the low-density pellet data from this form emphasizes its limitation to cases of Knudsen pore diffusion.

A steady state analysis shows that several mechanisms of both the Bonhoeffer-Farkas and Rideal-Eley types lead to the same kinetic form as the Langmuir-Hinshelwood formulation, which is properly limited to mechanisms of the Bonhoeffer-Farkas type.

Activation energies for the powdered

catalysts ranged from 1.6 to 10.4 kcal/mole with decreasing catalyst activity. The compensation effect noted is associated with variation in activation procedures with the different catalyst samples. The wide range of activation energies emphasizes the hazard in deriving conclusions as to mechanism on the basis of activation energies.

The 3.15-mm pellets in steel rings gave effectiveness factors smaller than 0.1. Using physical data on the catalyst and the measured effectiveness factors, calculated "tortuosities" for the high-density pellets fell in the reasonable range of 0.7 to 3.7. Activation energies for the pelleted catalysts fell within a narrower range than for the powders of similar activation histories. This difference is explained as being due to the effect of pore diffusion.

Acknowledgments

The authors acknowledge financial support for this program from the National Science Foundation, Grant G21-442, and fellowships to W.R.A. from the Eastman Kodak Co. and the Standard Oil Corp. of New Jersey. Appreciation is extended to S. K. Saraf for help with catalyst fabrication, and to G. W. Hendricks of the Union Oil Co. for physical measurements.

APPENDIX

Derivation of Kinetic Expression for Mechanisms 1 and 2 (Table 1) by Steady State Analysis

The derivation is for Mechanism 2. Mechanism 1 is shown to be a special case, and the related Langmuir-Hinshelwood solution is a further special case.

NET REACTION:

$$p(g) \rightarrow o(g)$$

MECHANISM:

$$p(g) \underset{k_{-4}}{\overset{k_4}{\rightleftarrows}} p(s)$$

$$o(g) \underset{k_{-4}}{\overset{k_4}{\rightleftarrows}} o(s)$$

$$p(s) + M \underset{k_{-1}}{\overset{k_1}{\rightleftarrows}} {}^{p}M$$

$$o(s) + M \underset{k_{-1}}{\overset{k_1}{\rightleftarrows}} {}^{o}M$$

$$p\,M \underset{k_2}{\overset{k_3}{\rightleftarrows}} o\,M$$

ASSUMPTIONS AND DEFINITIONS:

1. The two species have the same adsorption and desorption rate coefficients (as indicated above).

2. The ratio of the surface conversion rate coefficients is equal to the equilibrium constant, or

$$K_e = k_3/k_2 = c_{oe}/c_{pe} \qquad (A1)$$

3. The total hydrogen concentration in the gas phase is

$$c_t = c_p + c_o = c_{pe} + c_{oe} \qquad (A2)$$

4. c_m, c_{mp}, and c_{mo} are surface concentrations (as equivalent moles/cm^2) of empty sites, and of sites occupied by p-H_2 and o-H_2; the total active site concentration, c_{mt}, is a constant for a given catalyst and temperature:

$$c_{mt} = c_m + c_{mp} + c_{mo} \qquad (A3)$$

Similarly c_{pa} and c_{oa} are concentrations of the molecularly adsorbed (nonspecific as to sites) hydrogen, designated (s) in the mechanism.

5. $K_1 = k_1/k_{-1}$; $K_4 = k_4/k_{-4}$.

6. The main assumption is that the several surface concentrations do not vary with time.

DERIVATION:

The net reaction rate (per unit weight of catalyst) is

$$r/W = k_4c_p - k_{-4}c_{pa} \qquad (A4)$$

Balances are made on four surface species:

$$dc_{pa}/dt = 0 = k_{-1}c_{mp} + k_4c_p - k_1c_{pa}c_m - k_{-4}c_{pa} \qquad (A5)$$

$$dc_{oa}/dt = 0 = k_{-1}c_{mo} + k_4c_o - k_1c_{oa}c_m - k_{-4}c_{oa} \qquad (A6)$$

$$dc_{mp}/dt = 0 = k_1c_{pa}c_m + k_2c_{mo} - k_{-1}c_{mp} - k_3c_{mp} \qquad (A7)$$

$$dc_{mo}/dt = 0 = k_1c_{oa}c_m + k_3c_{mp} - k_{-1}c_{mo} - k_2c_{mo} \qquad (A8)$$

We wish to find r in terms of c_p, c_o, and c_{mt}. The five equations (A3) and (A5) to (A8)

have five "unknowns": c_m, c_{mp}, c_{mo}, c_{pa}, and c_{oa}. Thus c_{pa} may be found in terms of c_p, c_o, and c_{mt} and substituted into (A4). Then with the definitions (A1) and (A2), one obtains

$$\frac{r}{W(c_p - c_{pe})} = \frac{c_{mt}K_1K_4k_2(K_e + 1)}{[1 + K_1K_4c_t][1 + (k_2/k_{-1})(K_e + 1)] + [(k_2/k_{-4})(K_e + 1)K_1c_{mt}]} \quad \text{(A9)}$$

The right-hand side is the reaction rate coefficient K_r. It may be seen that

$$1/K_r = a(1 + b_1c_t) + b_2 \quad (4)$$

where $a \propto 1/c_{mt}$ and b_1 and b_2 are independent of c_{mt}.

The expression for Mechanism 1 may be simply derived from (A9) by letting the coefficients k_4 and k_{-4} be infinite. Then $K_4 \to 1$, $k_2/k_{-4} \to 0$, and

$$\frac{r}{W(c_p - c_{pe})} = \frac{c_{mt}K_1k_2(K_e + 1)}{[1 + K_1c_t][1 + (k_2/k_{-1})(K_e + 1)]} \quad \text{(A10)}$$

whence

$$1/K_r = a(1 + bc_t) \quad (3)$$

To obtain the "Langmuir-Hinshelwood" solution for Mechanism 1, assume that the adsorption and desorption steps are in equilibrium. Then the rate of desorption is much greater than the rate of conversion, and $k_{-1} \gg k_2$.

From (A10)

$$\frac{r}{W(c_p - c_{pe})} = \frac{c_{mt}K_1k_2(K_e + 1)}{1 + K_1c_t} \quad \text{(A11)}$$

which also has the form of Eq. (3).

References

1. Bond, G. C., "Catalysis by Metals." Academic Press, New York and London, 1962.
2. Bonhoeffer, K. F., and Farkas, A., *Z. Physik. Chem.* **B12**, 231 (1931).
3. Boreskov, G. K., and Vassilevitch, A. A., *Actes Congr. Intern. Catalyse, 2e, Paris, 1960,* p. 1095 (Éditions Technip, Paris, 1961).
4. Boudart, M., *Chem. Eng. Progr.* **58**, No. 7, 73 (1962).
5. Couper, A., and Eley, D. D., *Discussions Faraday Soc.* **172** (1950).
6. Couper, A., and Eley, D. D., *Proc. Roy. Soc. (London)* **A211**, 536 (1952).
7. Cremer, E., *Advan. Catalysis* **3**, 75 (1955).
8. Eley, D. D., and Rossington, D. R., *in* "Chemisorption, Proc. Symp. Keele, 1956" (W. E. Garner, ed.), p. 137. Butterworths, London, 1957.
9. Eley, D. D., and Shooter, D., *J. Catalysis* **2**, 259 (1963).
10. Harteck, P., and Schmidt, H. W., *Z. Physik. Chem.* **21**, 447 (1933).
11. Holden, S. J., and Rossington, D. R., *J. Phys. Chem.* **68**, 1061 (1964).
12. Holden, S. J., and Rossington, D. R., *J. Catalysis* **4**, 403 (1965).
13. Keeler, R. N., Weitzel, D. H., Blake, J. H., and Konecnik, M., *Advan. Cryogenic Engineering* **5**, 511 (Plenum Press, New York, 1960).
14. Kiperman, S. L., and Davydova, I. R., *Kinetika i Kataliz* **2**, 762 (1961).
15. Laidler, K. J., "Chemical Kinetics," p. 183. McGraw-Hill, New York, 1950.
16. Rao, M. R., and Smith, J. M., *A.I.Ch.E. J.* **9**, 485 (1963).
17. Rao, M. R., and Smith, J. M., *A.I.Ch.E. J.* **10**, 293 (1964).
18. Rao, M. R., Wakao, N., and Smith, J. M., *Ind. Eng. Chem. Fundamentals* **3**, 127 (1964).
19. Rideal, E. K., *Proc. Cambridge Phil. Soc.* **35**, 130 (1939).
20. Satterfield, C. N., and Saraf, S. K., *Ind. Eng. Chem. Fundamentals* **4**, 451 (1965).
21. Satterfield, C. N., and Sherwood, T. K., "The Role of Diffusion in Catalysis." Addison-Wesley, Reading, Massachusetts, 1963.
22. Schwab, G. M., and Killmann, E., *Actes Congr. Intern. Catalyse, 2e, Paris, 1960,* p. 1047 (1961).
23. Thiele, E. W., *Ind. Eng. Chem.* **31**, 916 (1939).
24. Wakao, N., Selwood, P. W., and Smith, J. M., *A.I.Ch.E. J.* **8**, 478 (1962).
25. Wicke, E., and Brötz, W., *Chem. Ing. Tech.* **21**, 219 (1949).